JACS
JOURNAL OF THE AMERICAN CHEMICAL SOCIETY
pubs.acs.org/JACS
Communication

In Crystallo Snapshots of Rh_2-Catalyzed C−H Amination

Anuvab Das, Chen-Hao Wang, Gerard P. Van Trieste III, Cheng-Jun Sun, Yu-Sheng Chen, Joseph H. Reibenspies, and David C. Powers*

Cite This: https://dx.doi.org/10.1021/jacs.0c09842
Read Online
ACCESS | Metrics & More | Article Recommendations | Supporting Information

ABSTRACT: While X-ray crystallography routinely provides structural characterization of kinetically stable pre-catalysts and intermediates, elucidation of the structures of transient reactive intermediates, which are intimately engaged in bond-breaking and -making during catalysis, is generally not possible. Here, we demonstrate *in crystallo* synthesis of Rh_2 nitrenoids that participate in catalytic C−H amination, and we characterize these transient intermediates as triplet adducts of Rh_2. Further, we observe the impact of coordinating substrate, which is present in excess during catalysis, on the structure of transient Rh_2 nitrenoids. By providing structural characterization of authentic C−H functionalization intermediates, and not kinetically stabilized model complexes, these experiments provide the opportunity to define critical structure−activity relationships.

X-ray and electron diffraction-based experiments are routinely employed to elucidate the chemical structures that are required for the rational design and optimization of small-molecule catalysts.[1,2] While crystallography is routinely utilized to examine ligand-induced structural variation in kinetically stable coordination complexes and pre-catalysts, application to the characterization of reactive intermediates, which are intimately involved in the bond-making and -breaking in catalysis, is typically stymied by the kinetic lability of these species.[3−7] As a result, experimental evaluation of the impact of ligand structure and coordinating additives present during catalysis is typically not possible.

Nitrene transfer catalysis represents a leading approach for the construction of C−N bonds via C−H amination and olefin aziridination reactions (Figure 1a).[8−25] Despite the ubiquity of Rh_2 nitrenoid intermediates in nitrene transfer catalysis, the structures of Rh_2 nitrenoids that participate in C−H amination have eluded experimental scrutiny. We have been interested in the characterization of transient intermediates involved in C−H functionalization reactions enabled by *in crystallo* synthesis.[26] This approach represents a crystalline analogue of classic matrix isolation experiments.[27−32] In 2019, we demonstrated that *in crystallo* N_2 extrusion from a Rh_2 adamantyl azide complex enabled structural characterization of a transient triplet nitrenoid adduct of Rh_2; however, rearrangement of the nitrene fragment prevented observation of C−H amination in this system (Figure 1b).[33] We hypothesized that generation of a Rh_2 nitrenoid bearing a proximal C−H bond would enable characterization of transient nitrene intermediates that were competent intermediates for intramolecular C−H amination (Figure 1c). Here, we report the characterization of a pair of transient Rh_2 nitrenoids that participate in solid-state C−H amination. These structural snapshots of a C−H amination reaction provide an opportunity to directly evaluate the impact of coordinating ligands on the structure of reactive intermediates in C−H functionalization.

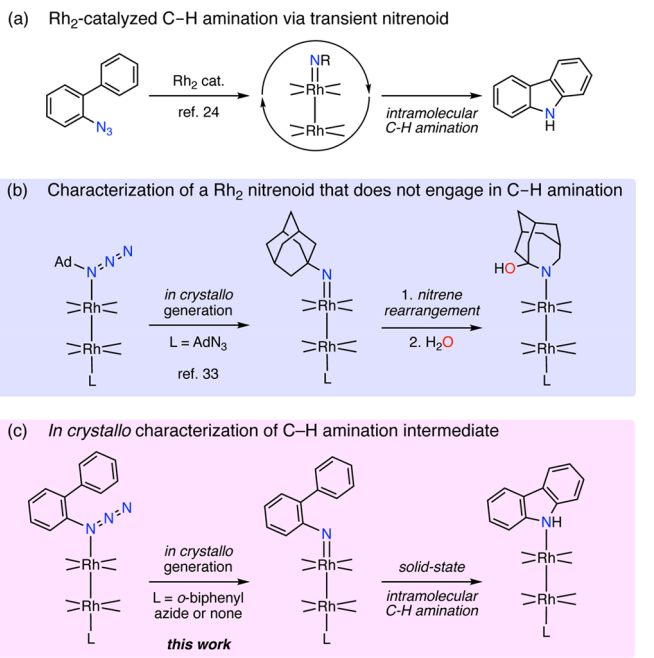

Figure 1. (a) Rh_2-catalyzed intramolecular nitrene transfer via transient Rh_2 nitrenoid intermediates. (b) *In situ* generation of a Rh_2 adamantyl nitrenoid enables crystallographic characterization; rapid rearrangement prevents C−H functionalization. (c) Characterization of transient Rh_2 nitrenoids enables observation of the impact of coordinating ligands on reactive amination intermediates.

Received: September 19, 2020

We initiated our studies by examining the coordination chemistry of $Rh_2(esp)_2$ (**1**) with *o*-biphenyl azide (**2**) (esp = *α,α,α′,α′*-tetramethyl-1,3-benzenedipropionate). These substrates were selected because $Rh_2(esp)_2$ (**1**) is among the most widely used catalysts for nitrene transfer chemistry, and *o*-biphenyl azides have been shown to participate in intramolecular amination.[24] An equimolar mixture of **1** and **2** in $CDCl_3$ displays ^{1}H NMR spectral features consistent with a 1:1 adduct (i.e., **3a**, Figure 2a, Figures S1 and S2). IR analysis of **3a** in a KBr pellet displays azide stretching modes at 2129 and 2101 cm^{-1} (for comparison, 2125 and 2089 cm^{-1} in **2**) (Figure S3). Single crystals of **3a** were obtained by slow evaporation of a CH_2Cl_2 solution of a 1:1 mixture of **1** and **2** at −35 °C (Figure 2b). The metrical parameters of the Rh_2 fragment and the biphenyl azide moiety in **3a** are similar to those of $Rh_2(esp)_2$ (Rh−Rh: **1** = 2.3817(9) Å; **3a** = 2.3850(4) Å) and **2**, respectively.[20,34]

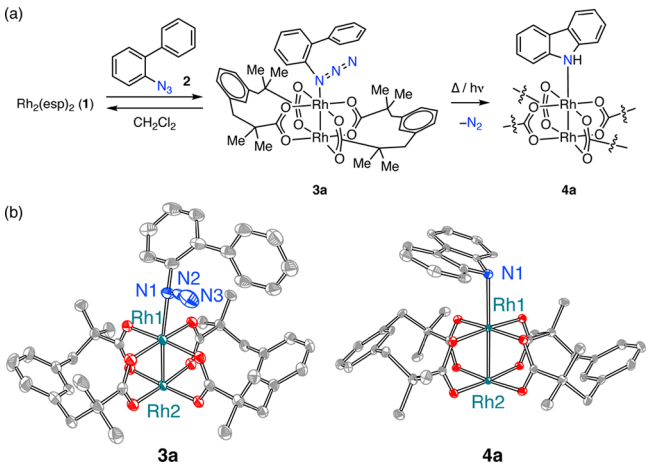

Figure 2. (a) Synthesis and reaction chemistry of Rh_2 complex **3a**. (b) Displacement ellipsoid plots of **3a** and **4a** (50% probability). H-atoms and solvent are omitted. Selected metrics: for **3a**, Rh(1)−N(1) = 2.244(3) Å, N(1)−C(1) = 1.441(5) Å, Rh(1)−Rh(2) = 2.3850(4) Å, Rh(1)−N(1)−C(1) = 125.0(2)°; for **4a**, Rh(1)−N(1) = 2.341(3) Å, Rh(1)−Rh(2) = 2.3835(3) Å.

Complex **3a** participates in solid-state, intramolecular C−H amination. Either photolysis ($335 < \lambda < 610$ nm) or thermolysis (60 °C) of a KBr pellet of complex **3a** results in the formation of carbazole complex **4a** (Figure 2b).[35] Solid-state conversion was evidenced by the disappearance of the stretching frequencies at 2129 and 2101 cm^{-1} and the appearance of peaks at 726, 575, and 508 cm^{-1} (Figures S6 and S7).[36] The final IR spectrum overlays with that of an authentic sample of **4a** prepared by treatment of $Rh_2(esp)_2$ with carbazole (Figures S11 and S12). The formation of **4a** was further confirmed by ^{1}H NMR following extraction of photolyzed or thermolyzed KBr pellets with $CDCl_3$ (Figures S13 and S14).

Intramolecular C−H amination within the coordination sphere of **3a** to generate **4a** presumably proceeds via Rh_2 nitrenoid **5a** (Figure 3a). Evidence of facile N_2 elimination from **3a** was obtained from flux-dependent matrix-assisted laser desorption/ionization mass spectrometry (MALDI-MS) measurements (Figure 3b). A signal corresponding to $Rh_2(esp)_2^+$ (m/z = 758.3599, calcd 758.0828) was observed at low laser power; as the flux of the ablation laser was increased, a new signal corresponding to the nitrenoid fragment $Rh_2(esp)_2(C_{12}H_{10}N)^+$ (m/z = 924.5538, calcd 925.1563) emerged.

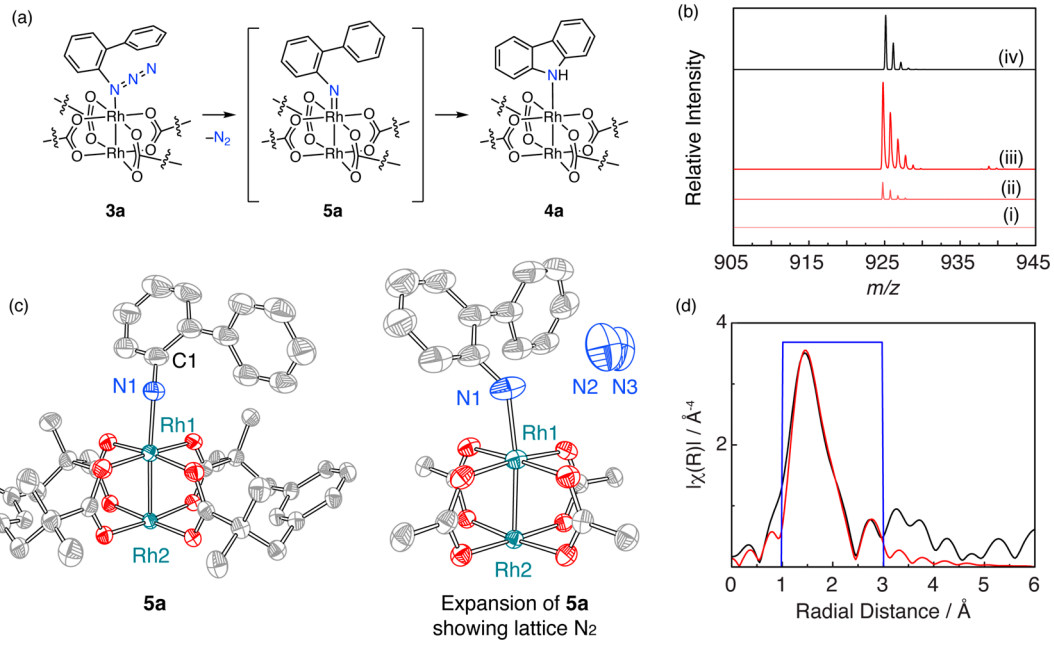

Figure 3. (a) Conversion of Rh_2 azide complex **3a** to carbazole adduct **4a** proceeds via transient Rh_2 nitrenoid **5a**. (b) Flux-dependent MALDI-MS shows an ion corresponding to $Rh_2(esp)_2(C_{12}H_{10}N)^+$; ablation laser flux increased from (i) to (iii). (iv) Simulated isotopic distribution for $Rh_2(esp)_2(C_{12}H_{10}N)^+$. (c) Left: Displacement ellipsoid plot of **5a** (50% probability). H-atoms, N_2, and solvent are omitted. Right: Rotated ellipsoid plot of **5a** (50% probability). H-atoms, esp ligand, and solvent are omitted. Selected metrics: Rh(1)−N(1) = 2.055(4) Å, N(1)−C(1) = 1.335(7) Å, Rh(1)−Rh(1) = 2.3953(4) Å, Rh(1)−N(1)−C(1) = 140.6(4)°. (d) Rh K-edge EXAFS data (spectral fitting range 1.0−3.0 Å, blue trace) of $Rh_2(esp)_2(C_{12}H_9N)$ (**5a**, experimental, black trace, and fit data, red trace).

https://dx.doi.org/10.1021/jacs.0c09842
J. Am. Chem. Soc. XXXX, XXX, XXX−XXX

Photolysis (λ = 365 nm) of a single crystal of **3a** under cryogenic conditions (100 K) promoted *in crystallo* synthesis of Rh_2 nitrenoid **5a**·N_2 (Figure 3c). Reaction progress was monitored by periodic collection of X-ray crystal structures (synchrotron radiation, λ = 0.41328 Å). Refinement of the resulting data indicated that the extrusion of N_2 generates Rh_2 nitrenoid **5a**·N_2 with 90% chemical conversion (Figure 3c).[37] Elimination of N_2 from **3a** is accompanied by the contraction of Rh(1)−N(1) from 2.244(3) Å (**3a**) to 2.055(4) Å (**5a**·N_2). Concurrently, contraction of N(1)−C(1) from 1.441(5) Å to 1.335(7) Å and expansion of the Rh(1)−N(1)−C(1) bond angle from 125.0(2)° to 140.6(4)° are observed.[38] The Rh(1)−Rh(2) bond distance remained unchanged (**3a**: 2.3850(4) Å, **5a**·N_2: 2.3953(4) Å). The evolved N_2 was refined at 90% occupancy, which is consistent with the single-crystal-to-single-crystal chemical conversion of the azide fragment in **3a** to the nitrene fragment in **5a**. *In crystallo* conversion of **3a** to **5a**·N_2 could also be accomplished more slowly by sustained exposure to synchrotron radiation (λ = 0.41328 Å) without photolysis. This observation is similar to X-ray-stimulated N_2 extrusion reactions previously observed in both Rh_2-[33] and Co-azide[39] complexes, and other X-ray stimulated reactions.[2] We were not able to observe conversion of **5a**·N_2 to **4a** via a second single-crystal-to-single-crystal transformation; slow warming of a crystal of **5a**·N_2 to promote C−H amination resulted in sample amorphization.

To further probe the structure of **5a**, Rh K-edge extended X-ray absorption fine structure (EXAFS) analysis was pursued. Data obtained for nitrenoid **5a** (generated by sustained (2 h) exposure of a boron nitride pellet of **3a** to synchrotron radiation (λ = 0.41328 Å)) was fit with four and half Rh−N/O interactions (2.03(1) Å) and one Rh−Rh interaction (2.401(6) Å) (Figure S16 and Table S6).[40,41] The first-shell Rh−N/O scatters were not distinguishable due to the limited resolution (0.22 Å = $\pi/(2\Delta k)$). These metrical parameters are consistent with those obtained from *in crystallo* synthesis of **5a**·N_2. Comparison of the X-ray absorption near-edge structure (XANES) data of $Rh_2(esp)_2$, **3a**, and **5a** suggests that all complexes feature a Rh_2[II,II] core (Figure S17).

The experimental metrical parameters of **5a** are in excellent agreement with density functional theory (DFT) optimization of the triplet electronic configuration (i.e., ^{3}[**5a**]) carried out at the wB97XD[42]/SDD (Rh)[43−45] and 6-31G(d) (light atoms)[46,47] levels of theory.[48] Consistent with the assigned electronic configuration, $\Delta E_{\text{triplet-singlet}}$ = −12.2 kcal·mol^{-1}. Comparison of various computational strategies that have been used in the past to examine Rh_2-catalyzed reactions revealed that while the optimized structures of **1** and **3a** were well captured by several methods, the optimized geometry of reactive intermediate **5a** displayed significant variation (Tables S7−S9).

During catalysis, substrate **2** is present in significant excess with respect to Rh_2 catalyst **1**.[24] Slow evaporation of a $CHCl_3$ solution of **1** that contained excess **2** afforded single crystals of **3b**, in which each Rh center is coordinated by an azide ligand (Figure 4). The metrical parameters of complexes **3a** and **3b** are similar except the Rh(1)−N(1) bond distance in **3b** (2.280(4) Å) is longer than the corresponding distance in **3a** (2.244(3) Å), which is consistent with a significant structural *trans* influence of the coordinated azide ligand.

Similar to **3a**, bis-azide complex **3b** participates in photochemically (335 < λ < 610 nm) and thermally (60 °C) promoted solid-state, intramolecular C−H amination. IR

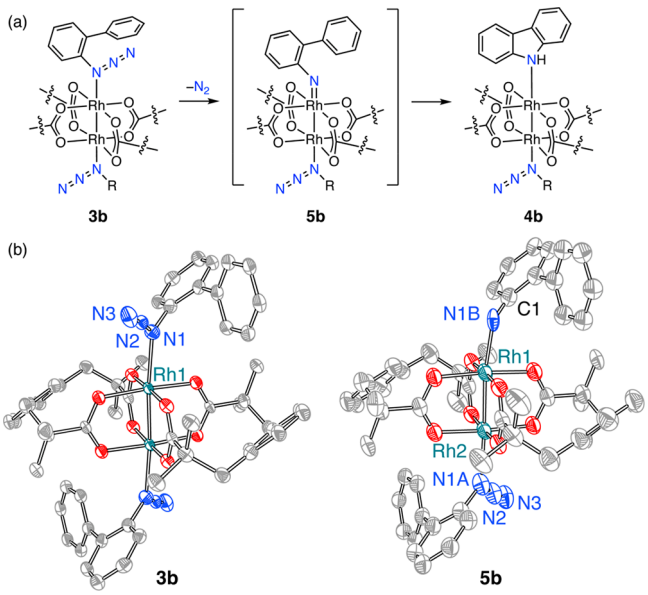

Figure 4. (a) Synthesis and photochemistry of Rh_2 bis-azide **3b**. (b) Displacement ellipsoid plots of **3b** and **5b** (50% probability). H-atoms and solvent are omitted. Selected metrics: for **3b**, Rh(1)−N(1) = 2.280(4) Å, N(1)−C(1) = 1.436(6) Å, Rh(1)−Rh(1) = 2.3872(6) Å, Rh(1)−N(1)−C(1) = 125.1(3)°; for **5b**, Rh(1)−N(1) = 2.10(4) Å, N(1)−C(1) = 1.36(4) Å, Rh(1)−Rh(1) = 2.4061(8) Å, Rh(1)−N(1)−C(1) = 127(2)°.

spectra obtained during either photolysis or thermolysis of a KBr pellet of **3b** revealed the disappearance of signals at 2129 and 2101 cm^{-1} and the evolution of new peaks at 726, 575, and 508 cm^{-1} (Figures S18 and S19). ^{1}H NMR analysis following extraction of either the photolyzed or thermolyzed KBr pellet with $CDCl_3$ revealed a 2:1 ratio of carbazole to $Rh_2(esp)_2$ (Figures S13 and S20), which indicates that both azide ligands undergo cyclization to carbazole under these conditions.

In crystallo expulsion of N_2 from **3b** enabled characterization of Rh_2 nitrenoid **5b**·N_2, which differs from **5a**·N_2 by the presence of a coordinated *o*-biphenylazide ligand on the distal Rh center (Figure 4b). *In crystallo* reaction progress was monitored by periodic collection of X-ray crystal structures. Refinement of the resulting data indicated that the extrusion of N_2 generated Rh_2 nitrenoid **5b**·N_2 in 43% chemical conversion (Figure 4).[49] The Rh centers in both **3b** and **5b**·N_2 are symmetry equivalent, and thus loss of N_2 results in positional disorder of the unreacted biphenyl azide and newly generated biphenyl nitrene moieties (i.e., each Rh center modeled as 50% $C_{12}H_{10}N_3$ and $C_{12}H_{10}N$ occupancy). Extrusion of N_2 from **3b** resulted in the contraction of Rh(1)−N(1) from 2.280(4) Å (**3b**) to 2.10(4) Å (**5b**·N_2). Concurrent with the expulsion of N_2 and the contraction of the Rh(1)−N(1) bond, N(1)−C(1) contracted from 1.436(6) Å to 1.36(4) Å and the Rh(1)−N(1)−C(1) bond angle expanded from 125.1(3)° to 127(2)°.[38] The Rh(1)−Rh(1) bond distance remained essentially unchanged (i.e., 2.3872(6) Å (**3b**); 2.4061(8) Å (**5b**·N_2)). We were unable to locate the evolved N_2 in the structure of **5b** due to disorder with a lattice $CHCl_3$. Crystallinity was compromised at higher chemical conversions, which prevented higher precision data from being obtained for **5b**.

DFT geometry optimization of ^{3}[**5b**] is well-matched to the experimental data and $\Delta E_{\text{triplet-singlet}}$ = −16.8 kcal·mol^{-1}. The

https://dx.doi.org/10.1021/jacs.0c09842
J. Am. Chem. Soc. XXXX, XXX, XXX−XXX

only significant deviation between experiment and theory is the bond angle, which is measured to be 127(2)° and computed to be 148.4° (consistent across computational methods examined, Tables S10−S12). We hypothesize that the observed deviation arises from crystal packing restrictions on *in crystallo* structural reorganization, which prevent full relaxation of the Rh−N−C angle in **5b**. Consistent with this hypothesis, the energy to bend the nitrene linkage on the triplet surface is <2 kcal·mol^{-1} (Table S13).

Comparison of the experimental structures of **5a**·N_2 and **5b**·N_2 reveals the impact of coordinated axial ligands on the reactive intermediate responsible for intramolecular C−H amination. In the absence of a trans axial ligand to the nitrene in **5a**, the Rh(1)−N(1) bond is 2.055(4) Å; in the presence of a trans axial azide ligand to the nitrene in **5b**, the Rh(1)−N(1) bond distance is 2.10(4) Å. The long Rh−N linkage in **5b** suggests a significant structural *trans* effect through the M−M bond (Table S14).[50−54] In addition to elongating the Rh−nitrenoid bond, the presence of an axial ligand increases the spin density on the nitrene nitrogen atom: natural bond order (NBO) analysis of ^{3}[**5a**] and ^{3}[**5b**] indicates the N-centered spin density increases upon azide binding (**5a**, 1.16 e$^-$; **5b**, 1.48 e$^-$) (Figure 5, Tables S15 and S16).

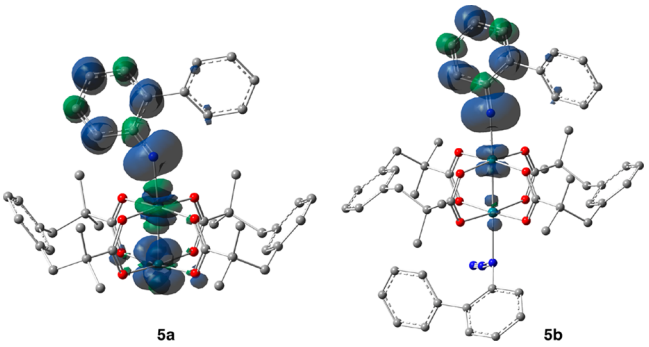

Figure 5. Calculated spin density plots for Rh_2 nitrenoid complexes ^{3}[**5a**] and ^{3}[**5b**]; isolevel = 0.004.

In summary, we describe the structural characterization of a pair of Rh_2 nitrenes that mediate intramolecular C−H amination chemistry. *In crystallo* confinement enables direct characterization of the species that are intimately involved in bond-breaking and -making in catalysis. Importantly, by having access to experimentally derived metrical parameters, we were able to evaluate the fidelity of various commonly employed computational approaches to the description of Rh_2-catalyzed processes, which provides critical but previously unavailable insight into the fidelity of these models to experiment. These observations demonstrate *in situ* crystallography to be a powerful tool for characterizing authentic C−H activation intermediates.

■ ASSOCIATED CONTENT

Supporting Information

The Supporting Information is available free of charge at https://pubs.acs.org/doi/10.1021/jacs.0c09842.

Synthesis and characterization of the compounds described herein, including Figures S1−S35 and Tables S1−S27 (PDF)

Crystallographic data for **3a**, **3b**, **4a**, **5a**, and **5b** (also available free of charge from the Cambridge Crystallographic Data Center under CCDC 2025847−2025851) (TXT)

■ AUTHOR INFORMATION

Corresponding Author

David C. Powers − *Department of Chemistry, Texas A&M University, College Station, Texas 77843, United States;* orcid.org/0000-0003-3717-2001; Email: powers@chem.tamu.edu

Authors

Anuvab Das − *Department of Chemistry, Texas A&M University, College Station, Texas 77843, United States;* orcid.org/0000-0002-9344-4414

Chen-Hao Wang − *Department of Chemistry, Texas A&M University, College Station, Texas 77843, United States;* orcid.org/0000-0003-3416-4452

Gerard P. Van Trieste III − *Department of Chemistry, Texas A&M University, College Station, Texas 77843, United States*

Cheng-Jun Sun − *Advanced Photon Source, Argonne National Laboratory, Argonne, Illinois 60439, United States*

Yu-Sheng Chen − *ChemMatCARS, University of Chicago, Argonne, Illinois 60439, United States*

Joseph H. Reibenspies − *Department of Chemistry, Texas A&M University, College Station, Texas 77843, United States*

Complete contact information is available at: https://pubs.acs.org/10.1021/jacs.0c09842

Notes

The authors declare no competing financial interest.

■ ACKNOWLEDGMENTS

The authors thank Yohannes H. Rezenom for assisting with the MALDI experiment and Debmalya Ray for helpful discussion. X-ray diffraction data of **3a**, **3b**, **5a**·N_2, and **5b**·N_2 were collected at ChemMatCARS Sector 15 housed at Advanced Photon Source (APS) at Argonne National Laboratory (ANL), which is supported by the National Science Foundation (NSF), Division of Chemistry (CHE), and Materials Research (DMR) (NSF/CHE-1346572). Use of the PILATUS X CdTe 1M detector is supported by NSF (NSF/DMR-1531283). XANES/EXAFS data of **1**, **3a**, and **5a** were collected at Beamline 20-ID housed at APS. This research used resources of the Advanced Photon Source, an Office of Science User Facility operated for the U.S. Department of Energy (DOE) Office of Science by Argonne National Laboratory, and was supported by the U.S. DOE under Contract No. DE-AC02-06CH11357, and the Canadian Light Source and its funding partners. The authors acknowledge the U.S. DOE, Office of Science, Office of Basic Energy Sciences, Catalysis Program (DE-SC0018977), the Welch Foundation (A-1907), and an Alfred P. Sloan Fellowship to D.C.P. for financial support.

■ REFERENCES

(1) Jones, C. G.; Asay, M.; Kim, L. J.; Kleinsasser, J. F.; Saha, A.; Fulton, T. J.; Berkley, K. R.; Cascio, D.; Malyutin, A. G.; Conley, M. P.; Stoltz, B. M.; Lavallo, V.; Rodríguez, J. A.; Nelson, H. M. Characterization of Reactive Organometallic Species via MicroED. *ACS Cent. Sci.* **2019**, *5*, 1507−1513.

(2) Ohashi, Y.; Sasada, Y. X-ray Analysis of Co−C Bond Cleavage in the Crystalline State. *Nature* **1977**, *267*, 142−144.
(3) Das, A.; Van Trieste, G. P., III; Powers, D. C. Crystallography of Reactive Intermediates. *Comments Inorg. Chem.* **2020**, *40*, 116−158.
(4) Kornecki, K. P.; Briones, J. F.; Boyarskikh, V.; Fullilove, F.; Autschbach, J.; Schrote, K. E.; Lancaster, K. M.; Davies, H. M. L.; Berry, J. F. Direct Spectroscopic Characterization of a Transitory Dirhodium Donor-Acceptor Carbene Complex. *Science* **2013**, *342*, 351−354.
(5) Carsch, K. M.; DiMucci, I. M.; Iovan, D. A.; Li, A.; Zheng, S.-L.; Titus, C. J.; Lee, S. J.; Irwin, K. D.; Nordlund, D.; Lancaster, K. M.; Betley, T. A. Synthesis of a Copper-Supported Triplet Nitrene Complex Pertinent to Copper-Catalyzed Amination. *Science* **2019**, *365*, 1138−1143.
(6) Werlé, C.; Goddard, R.; Fürstner, A. The First Crystal Structure of a Reactive Dirhodium Carbene Complex and a Versatile Method for the Preparation of Gold Carbenes by Rhodium-to-Gold Transmetalation. *Angew. Chem., Int. Ed.* **2015**, *54*, 15452−15456.
(7) Rohde, J.-U.; In, J.-H.; Lim, M. H.; Brennessel, W. W.; Bukowski, M. R.; Stubna, A.; Münck, E.; Nam, W.; Que, L. Crystallographic and Spectroscopic Characterization of a Nonheme Fe(IV)=O Complex. *Science* **2003**, *299*, 1037−1039.
(8) Hennessy, E. T.; Betley, T. A. Complex N-Heterocycle Synthesis via Iron-Catalyzed, Direct C−H Bond Amination. *Science* **2013**, *340*, 591−595.
(9) Godula, K.; Sames, D. C.-H. Bond Functionalization in Complex Organic Synthesis. *Science* **2006**, *312*, 67−72.
(10) Ochiai, M.; Miyamoto, K.; Kaneaki, T.; Hayashi, S.; Nakanishi, W. Highly Regioselective Amination of Unactivated Alkanes by Hypervalent Sulfonylimino-λ^3-Bromane. *Science* **2011**, *332*, 448−451.
(11) Hong, S. Y.; Park, Y.; Hwang, Y.; Kim, Y. B.; Baik, M.-H.; Chang, S. Selective Formation of γ-lactams via C−H Amidation Enabled by Tailored Iridium Catalysts. *Science* **2018**, *359*, 1016−1021.
(12) Lei, H.; Rovis, T. A Site-Selective Amination Catalyst Discriminates between Nearly Identical C−H Bonds of Unsymmetrical Disubstituted Alkenes. *Nat. Chem.* **2020**, *12*, 725−731.
(13) Prier, C. K.; Zhang, R. K.; Buller, A. R.; Brinkmann-Chen, S.; Arnold, F. H. Enantioselective, Intermolecular Benzylic C−H Amination Catalysed by an Engineered Iron-Haem Enzyme. *Nat. Chem.* **2017**, *9*, 629−634.
(14) Yang, Y.; Cho, I.; Qi, X.; Liu, P.; Arnold, F. H. An Enzymatic Platform for the Asymmetric Amination of Primary, Secondary and Tertiary C(sp^3)−H Bonds. *Nat. Chem.* **2019**, *11*, 987−993.
(15) Clark, J. R.; Feng, K.; Sookezian, A.; White, M. C. Manganese-Catalysed Benzylic C(sp3)−H Amination for Late-Stage Functionalization. *Nat. Chem.* **2018**, *10*, 583−591.
(16) Davies, H. M. L.; Manning, J. R. Catalytic C−H functionalization by Metal Carbenoid and Nitrenoid Insertion. *Nature* **2008**, *451*, 417−424.
(17) Jiang, H.; Lang, K.; Lu, H.; Wojtas, L.; Zhang, X. P. Asymmetric Radical Bicyclization of Allyl Azidoformates via Cobalt(II)-Based Metalloradical Catalysis. *J. Am. Chem. Soc.* **2017**, *139*, 9164−9167.
(18) Jat, J. L.; Paudyal, M. P.; Gao, H.; Xu, Q.-L.; Yousufuddin, M.; Devarajan, D.; Ess, D. H.; Kürti, L.; Falck, J. R. Direct Stereospecific Synthesis of Unprotected N−H and N−Me Aziridines from Olefins. *Science* **2014**, *343*, 61−65.
(19) Paudyal, M. P.; Adebesin, A. M.; Burt, S. R.; Ess, D. H.; Ma, Z.; Kürti, L.; Falck, J. R. Dirhodium-Catalyzed C−H Arene Amination using Hydroxylamines. *Science* **2016**, *353*, 1144−1147.
(20) Espino, C. G.; Fiori, K. W.; Kim, M.; Du Bois, J. Expanding the Scope of C−H Amination through Catalyst Design. *J. Am. Chem. Soc.* **2004**, *126*, 15378−15379.
(21) Harrison, J. G.; Gutierrez, O.; Jana, N.; Driver, T. G.; Tantillo, D. J. Mechanism of Rh_2(II)-Catalyzed Indole Formation: The Catalyst Does Not Control Product Selectivity. *J. Am. Chem. Soc.* **2016**, *138*, 487−490.
(22) Nguyen, Q.; Sun, K.; Driver, T. G. Rh_2(II)-Catalyzed Intramolecular Aliphatic C−H Bond Amination Reactions Using Aryl Azides as the N-Atom Source. *J. Am. Chem. Soc.* **2012**, *134*, 7262−7265.
(23) Shen, M.; Leslie, B. E.; Driver, T. G. Dirhodium(II)-Catalyzed Intramolecular C−H Amination of Aryl Azides. *Angew. Chem., Int. Ed.* **2008**, *47*, 5056−5059.
(24) Stokes, B. J.; Jovanović, B.; Dong, H.; Richert, K. J.; Riell, R. D.; Driver, T. G. Rh_2(II)-Catalyzed Synthesis of Carbazoles from Biaryl Azides. *J. Org. Chem.* **2009**, *74*, 3225−3228.
(25) Stokes, B. J.; Dong, H.; Leslie, B. E.; Pumphrey, A. L.; Driver, T. G. Intramolecular C−H Amination Reactions: Exploitation of the Rh_2(II)-Catalyzed Decomposition of Azidoacrylates. *J. Am. Chem. Soc.* **2007**, *129*, 7500−7501.
(26) Das, A.; Reibenspies, J. H.; Chen, Y.-S.; Powers, D. C. Direct Characterization of a Reactive Lattice-Confined Ru_2 Nitride by Photocrystallography. *J. Am. Chem. Soc.* **2017**, *139*, 2912−2915.
(27) Kawano, M.; Sano, T.; Abe, J.; Ohashi, Y. The First in Situ Direct Observation of the Light-Induced Radical Pair from a Hexaarylbiimidazolyl Derivative by X-ray Crystallography. *J. Am. Chem. Soc.* **1999**, *121*, 8106−8107.
(28) Kawano, M.; Hirai, K.; Tomioka, H.; Ohashi, Y. Structure Analysis of a Transient Triplet Carbene Trapped in a Crystal. *J. Am. Chem. Soc.* **2001**, *123*, 6904−6908.
(29) Kawano, M.; Takayama, T.; Uekusa, H.; Ohashi, Y.; Ozawa, Y.; Matsubara, K.; Imabayashi, H.; Mitsumi, M.; Toriumi, K. Structure Analysis of Photo-induced Triplet Phenylnitrene Using Synchrotron Radiation. *Chem. Lett.* **2003**, *32*, 922−923.
(30) Novozhilova, I. V.; Volkov, A. V.; Coppens, P. Theoretical Analysis of the Triplet Excited State of the $[Pt_2(H_2P_2O_5)_4]^{4-}$ Ion and Comparison with Time-Resolved X-ray and Spectroscopic Results. *J. Am. Chem. Soc.* **2003**, *125*, 1079−1087.
(31) Sun, J.; Abbenseth, J.; Verplancke, H.; Diefenbach, M.; de Bruin, B.; Hunger, D.; Würtele, C.; van Slageren, J.; Holthausen, M. C.; Schneider, S. A Platinum(II) Metallonitrene with a Triplet Ground State. *Nat. Chem.* **2020**, *12*, 1054−1059.
(32) Shields, D. J.; Karothu, D. P.; Sambath, K.; Ranaweera, R. A. A. U.; Schramm, S.; Duncan, A.; Duncan, B.; Krause, J. A.; Gudmundsdottir, A. D.; Naumov, P. Cracking under Internal Pressure: Photodynamic Behaviour of Vinyl Azide Crystals through N_2 Release. *J. Am. Chem. Soc.* **2020**, *142*, 18565−18575.
(33) Das, A.; Chen, Y.-S.; Reibenspies, J. H.; Powers, D. C. Characterization of a Reactive Rh_2 Nitrenoid by Crystalline Matrix Isolation. *J. Am. Chem. Soc.* **2019**, *141*, 16232−16236.
(34) Takayama, T.; Mitsumori, T.; Kawano, M.; Sekine, A.; Uekusa, H.; Ohashi, Y.; Sugawara, T. Direct Observation of Arylnitrene Formation in the Photoreaction of Arylazide Crystals. *Acta Crystallogr., Sect. B: Struct. Sci.* **2010**, *66*, 639−646.
(35) The photolysis of **3a** could not be monitored in the solution phase by either UV−vis or NMR due to the facts that (1) *o*-biphenylazide (**2**) is a weakly bound ligand and (2) *o*-biphenylazide by itself has a background photochemistry to generate the carbazole (see Figures S4 and S5).
(36) The thermal decomposition of **3a** proceeds via first-order kinetics (see Figure S8 and Table S1). Monitoring temperature-dependent kinetics for thermolysis of **3a** provides E_a = 24.9 kcal·mol^{-1} for the thermally promoted intramolecular amination (see Figure S9 and Table S2).
(37) **3a**: $P2_1/n$, a = 10.712(2) Å, b = 12.937(2) Å, c = 32.667(4) Å, β = 96.259(3)°; **5a**·N_2: $P2_1/c$, a = 10.9316(8) Å, b = 12.9312(9) Å, c = 32.433(2) Å, β = 99.310(1)°.
(38) The contraction of the N−C bonds of the nitrene fragment in the generated Rh_2 nitrenoids **5a** and **5b** is due to delocalized double bond character (see Table S4).
(39) Baek, Y.; Das, A.; Zheng, S.-L.; Reibenspies, J. H.; Powers, D. C.; Betley, T. A. C.-H. Amination Mediated by Cobalt Organoazide Adducts and the Corresponding Cobalt Nitrenoid Intermediates. *J. Am. Chem. Soc.* **2020**, *142*, 11232−11243.

https://dx.doi.org/10.1021/jacs.0c09842
J. Am. Chem. Soc. XXXX, XXX, XXX−XXX

(40) For Rh K-edge EXAFS analysis of azide adduct **3a**, see Figure S15 and Table S5.
(41) Analysis of the edge energy and spectral intensity from successive measurements indicates that significant chemical conversion is not observed on the time scale of the experiment.
(42) Chai, J.-D.; Head-Gordon, M. Long-Range Corrected Hybrid Density Functionals with Damped Atom-Atom Dispersion Corrections. *Phys. Chem. Chem. Phys.* **2008**, *10*, 6615−6620.
(43) Andrae, D.; Häußermann, U.; Dolg, M.; Stoll, H.; Preuß, H. Energy-Adjusted *Ab Initio* Pseudopotentials for the Second and Third Row Transition Elements. *Theor. Chim. Acta* **1990**, *77*, 123−141.
(44) Cao, X.; Dolg, M. Valence Basis Sets for Relativistic Energy-Consistent Small-Core Lanthanide Pseudopotentials. *J. Chem. Phys.* **2001**, *115*, 7348−7355.
(45) Dolg, M.; Wedig, U.; Stoll, H.; Preuss, H. Energy-Adjusted *Ab Initio* Pseudopotentials for the First Row Transition Elements. *J. Chem. Phys.* **1987**, *86*, 866−872.
(46) Petersson, G. A.; Al-Laham, M. A. A Complete Basis Set Model Chemistry. II. Open-Shell Systems and the Total Energies of the First-Row Atoms. *J. Chem. Phys.* **1991**, *94*, 6081−6090.
(47) Petersson, G. A.; Bennett, A.; Tensfeldt, T. G.; Al-Laham, M. A.; Shirley, W. A.; Mantzaris, J. A Complete Basis Set Model Chemistry. I. The Total Energies of Closed-Shell Atoms and Hydrides of the First-Row Elements. *J. Chem. Phys.* **1988**, *89*, 2193−2218.
(48) Wu, X.; Bao, X. Computational Insights into Different Chemoselectivities in Rh_2(II)-Catalyzed *N*-Aryl Nitrene and Analogous Rh_2(II)/Cu(I)-Catalyzed Aryl-Substituted Carbene Involving Reactions. *Catal. Sci. Technol.* **2019**, *9*, 1518−1527.
(49) During the *in crystallo* generation of **5b** from **3b**, the unit cell parameters changed from a = 12.881(2) Å, b = 12.949(2) Å, c = 18.331(3) Å, β = 102.871(2)°, and V = 2981.0(8) Å^3 to a = 12.961(2) Å, b = 12.909(2) Å, c = 18.381(3) Å, β = 100.334(2)°, and V = 3025.5(8) Å^3].
(50) Che, C.-M.; Lee, W.-M.; Mak, T. C. W.; Gray, H. B. Axial-Ligand and Metal-Metal Trans Influences in Binuclear Platinum(III) Complexes. Crystal Structures and Spectroscopic Properties of $K_4[Pt_2(P_2O_5H_2)_4(SCN)_2]\cdot 2H_2O$, $K_4[Pt_2(P_2O_5H_2)_4(NO_2)_2]\cdot 2KNO_2\cdot 2H_2O$, and $K_4[Pt_2(P_2O_5H_2)_4(C_3H_3N_2)_2]\cdot 7H_2O$. *J. Am. Chem. Soc.* **1986**, *108*, 4446−4451.
(51) Appleton, T. G.; Clark, H. C.; Manzer, L. E. The *trans*-Influence: Its Measurement and Significance. *Coord. Chem. Rev.* **1973**, *10*, 335−422.
(52) Alexander, K. A.; Bryan, S. A.; Fronczek, F. R.; Fultz, W. C.; Rheingold, A. L.; Roundhill, D. M.; Stein, P.; Watkins, S. F. Crystal and Molecular Structures of Dihalotetrakis(pyrophosphito)-diplatinum(III) Complexes. Integrative use of Structural and Vibrational Data to Assess Intermetallic Bonding and the Trans Influence of the Platinum(III)-Platinum(III) Bond. *Inorg. Chem.* **1985**, *24*, 2803−2808.
(53) Ariafard, A.; Hyland, C. J. T.; Canty, A. J.; Sharma, M.; Brookes, N. J.; Yates, B. F. Ligand Effects in Bimetallic High Oxidation State Palladium Systems. *Inorg. Chem.* **2010**, *49*, 11249−11253.
(54) Che, C.-M.; Cheng, M.-C.; Wang, Y.; Gray, H. B. *trans*-Effect of Dialkyl Sulfide on a Pt(III)-Pt(III) Bond. Synthesis, Spectroscopy and X-ray Crystal Structure of $[Bu_4N]_2[Pt_2(P_2O_5H_2)_4(SEt_2)_2]$. *Inorg. Chim. Acta* **1992**, *191*, 7−9.

https://dx.doi.org/10.1021/jacs.0c09842
J. Am. Chem. Soc. XXXX, XXX, XXX−XXX